TESLA LC-PHSM-2001-038
6 February, 2001

Strong Electroweak Symmetry Breaking Signals in WW Scattering at TESLA

Roberto Chierici*, **Stefano Rosati**† **and Michael Kobel**†

*CERN, CH-1211 Geneva 23, Switzerland
†Physikalisches Institut der Universität Bonn, D-53115 Bonn, Germany

Abstract

A realistic study of the processes $e^+e^- \to W^+W^-\nu\bar{\nu} \to q\bar{q}q\bar{q}\nu\bar{\nu}$ and $e^+e^- \to ZZ\nu\bar{\nu} \to q\bar{q}q\bar{q}\nu\bar{\nu}$ as probes for signals of strong electroweak symmetry breaking at TESLA energies is presented. Expected limits on the parameters α_4 and α_5 in the electroweak chiral Lagrangian, are given and discussed.

Introduction

The most outstanding problem in modern particle physics is how Nature realizes the breaking of the SU(2) $\otimes$ U(1) gauge symmetry. In the absence of a light scalar field, new physics coupled to the Standard Model (SM) is needed at the TeV scale to restore the unitarity of the model (see e.g. [1]). In particular a larger symmetry should exist, breaking down to SU(2) $\otimes$ U(1) and introducing the needed Goldstone bosons to give longitudinal components to W and Z, hence masses. The minimal way to realize this is via the breaking SU(2) $\otimes$ SU(2) $\rightarrow$ SU(2), which resembles the symmetry breaking pattern of QCD in the limit of zero quark masses. The pions of the new strong symmetry correspond to the Goldstone bosons used to give the longitudinal polarisation to W and Z. High energy boson scattering, decoupling transversal and longitudinal components, brings therefore information on the underlying dynamics of the new symmetry. WW scattering at low energies can be effectively described by the so-called chiral Lagrangian [2, 3], containing effective operators of increasing dimensions. Besides the gauge interactions, there are only two dimension-four interactions that respect the custodial SU(2), describing the scattering of two bosons; these terms depend upon two anomalous couplings, known in the literature as α_4 and α_5. The values of these couplings are model dependent, but both are equal to zero in the SM. The two dimension-four interaction terms can be written as:

$$L_4 = \frac{\alpha_4}{16\pi^2}\mathrm{tr}(V_\mu V_\nu)\mathrm{tr}(V^\mu V^\nu) \tag{1}$$

$$L_5 = \frac{\alpha_5}{16\pi^2}\mathrm{tr}(V_\mu V^\mu)\mathrm{tr}(V_\nu V^\nu) \tag{2}$$

where V_μ simplifies to -i$g\frac{\sigma^i}{2}W^i_\mu$ + i$g'\frac{\sigma^3}{2}B_\mu$ in the unitary gauge. The couplings α_4, α_5 are related to the scales of new physics Λ^*_4, Λ^*_5 by naive dimensional analysis [4]:

$$\frac{\alpha_i}{16\pi^2} = \left(\frac{v}{\Lambda^*_i}\right)^2 \tag{3}$$

where v=246 GeV is the Fermi scale, fixed by low energy weak interactions.
In what follows a study about the limits which can be set on α_4, α_5 at TESLA by studying $e^+e^- \rightarrow W^+W^-\nu\bar{\nu} \rightarrow q\bar{q}q\bar{q}\nu\bar{\nu}$ and $e^+e^- \rightarrow ZZ\nu\bar{\nu} \rightarrow q\bar{q}q\bar{q}\nu\bar{\nu}$ processes, is presented. A center of mass energy of 800 GeV and a total luminosity of 1000 fb^{-1} is assumed throughout this work. Beam polarisations of 80% for electrons and 40% for positrons are also assumed. This study completes and updates what has been presented in [5].

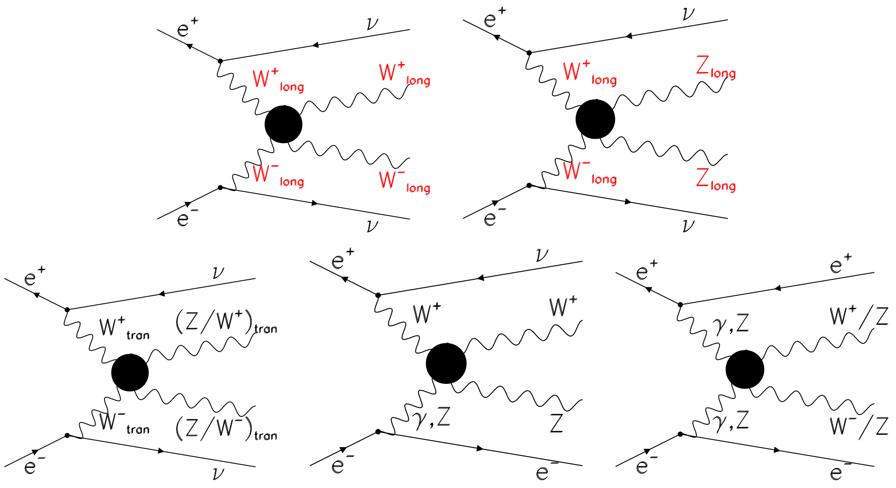

Figure 1: Diagrams contributing to longitudinal WW scattering and main six fermion backgrounds from doubly resonant processes.

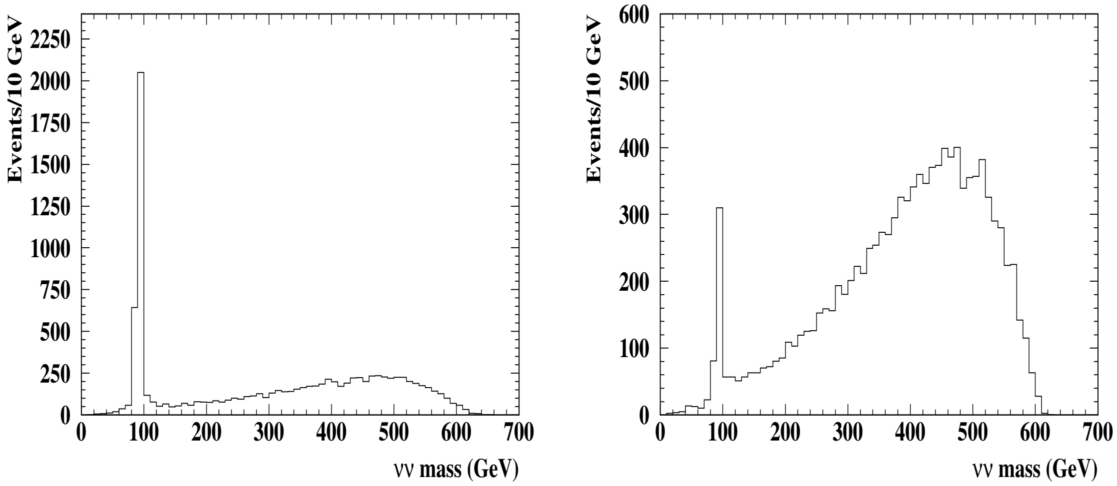

Figure 2: Invariant mass of the $\nu\nu$ system in $q\bar{q}q\bar{q}\nu\bar{\nu}$ generated events with the $q\bar{q}$ mass cuts for W (left) and Z (right) described in the text.

Table 1: Cross-sections of signal and background processes and programs used for the generation. Beam polarisations of 80% for electrons and 40% for positrons are also assumed. The $WW\nu\nu$ and $ZZ\nu\nu$ signals are defined with the cuts described in the text.

	Channel	$\sigma_{800\ GeV}$(fb)	Generator
6-f	$e^+e^- \to W^+W^-\nu\bar{\nu} \to q\bar{q}q\bar{q}\nu\bar{\nu}$	8.64	WHiZard
	$e^+e^- \to ZZ\nu\bar{\nu} \to q\bar{q}q\bar{q}\nu\bar{\nu}$	4.28	WHiZard
	$e^+e^- \to q\bar{q}q\bar{q}\nu\bar{\nu}$ (background)	5.5	WHiZard
	$e^+e^- \to WZe\nu \to q\bar{q}q\bar{q}e\nu$	39.2	WHiZard
	$e^+e^- \to W^+W^-e^+e^- \to q\bar{q}q\bar{q}e^+e^-$	286.4	WHiZard
	$e^+e^- \to ZZe^+e^- \to q\bar{q}q\bar{q}e^+e^-$	0.9	WHiZard
	$e^+e^- \to t\bar{t} \to X$	619	PYTHIA
4-f	$e^+e^- \to W^+W^- \to q\bar{q}q\bar{q}$	5900	PYTHIA
	$e^+e^- \to ZZ \to q\bar{q}q\bar{q}$	302	PYTHIA
2-f	$e^+e^- \to q\bar{q} \to X$	9180	PYTHIA

Analysis setup

Six fermion processes under study correspond to the longitudinal scattering of W bosons, namely the $ee \to W_lW_l\nu\nu$ and $ee \to Z_lZ_l\nu\nu$ processes. Figure 1 shows the signal and the main six-fermion backgrounds, coming from doubly resonant boson-boson scattering. The signal is also affected by four and two-fermion backgrounds. Only final states with four quarks are studied here.

For the generation of two and four-fermion final states PYTHIA [6] was used, whereas six-fermion signal and backgrounds were generated with WHiZard [7] using the O'Mega [8] matrix elements. Flavour independent $\ell\ell q\bar{q}q\bar{q}$ final states were built summing consistently independently generated samples with a defined quark configuration. As an example the six-fermion $e\nu q\bar{q}q\bar{q}$ final state is built as:

$$e\nu q\bar{q}q\bar{q} = 8 \cdot e^+\nu u\bar{u}s\bar{c} + 12 \cdot e^+\nu d\bar{d}s\bar{c} \qquad (4)$$

In table 1 the cross-sections at $\sqrt{s} = 800$ GeV of the relevant processes are reported, together with the program used for their generation. The hadronisation is realised by using JETSET [6].

The doubly resonant signals, $WW\nu\nu$ and $ZZ\nu\nu$, are defined with the following cuts on the $ee \to q\bar{q}q\bar{q}\nu\nu$ phase space:

$$\begin{gathered} 2m_X - 12\ GeV\ \le m^1_{qq} + m^2_{qq} \le\ 2m_X + 12\ GeV \\ |m^1_{qq} - m^2_{qq}| \le\ 20\ GeV \\ m_{\nu\nu} \ge\ 100\ GeV \end{gathered}$$

where X denotes a boson and the cut on the neutrinos invariant mass is to remove the contribution of WWZ and ZZZ production. Figure 2 shows the distribution,

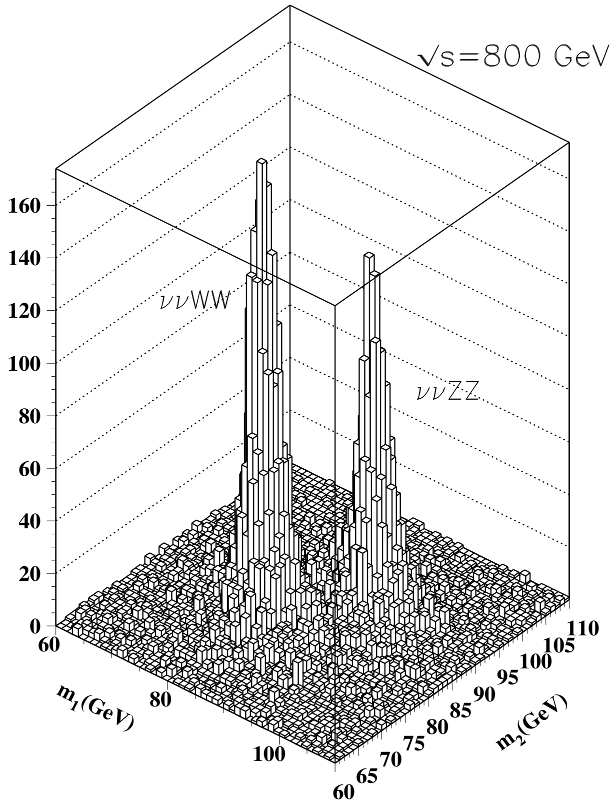

Figure 3: Reconstructed $q\bar{q}$ invariant masses after SIMDET on $WW\nu\nu$ and $\nu\nu ZZ$ events.

at generator level, of $m_{\nu\nu}$ after the application of the other mass cuts. The Z peak is evident and not contributing to boson-boson scattering processes.

The detector simulation is done with SIMDET v3.1 [9] in its default setup taken from the Tesla CDR [10]. Detector performance can be found there:

tracking: large TPC as main tracking device. CCD vertex detector with its first layer at 2 cm from the interaction point and a forward tracker to guarantee an overall tracking coverage down to 5 degrees. A magnetic field of 3 T is used.

calorimetry: electromagnetic calorimeter with resolution $\frac{\Delta E}{E}$ $=10\%/\sqrt{E}+0.6\%$, hadronic calorimeter with resolution $\frac{\Delta E}{E}$ $=40\%/\sqrt{E}+4\%$, total acceptance down to 5 degrees.

forward coverage: instrumented mask from 5 to 83 mrad without dead regions, Low Angle Tagger acceptance from 23.5 to 83.1 mrad [11].

The performances of the detector have been studied in terms of separation power of W from Z, using $ee \to WW\nu\nu$ and $ee \to ZZ\nu\nu$ events generated with GRACE [12] and hadronised with JETSET, to remove the six-fermion background contributions. The reconstructed mass peaks in the plane of the two masses after the inclusion of the detector simulation is shown in figure 3 and demonstrates an excellent separation of the two contributions at 800 GeV. This corresponds to a resolution in the invariant $q\bar{q}$ mass of 4%.

$ZZ\nu\nu$ selection

The selection can exploit the optimal forward coverage and mass resolution of the Tesla detector, to reject the following background classes:

- 4-fermion (WW, ZZ)
- 2-fermion ($q\bar{q}$ $t\bar{t}$)
- 6-fermion ($WW\nu\nu$, $WZe\nu$, $WWee$, $ZZee$)

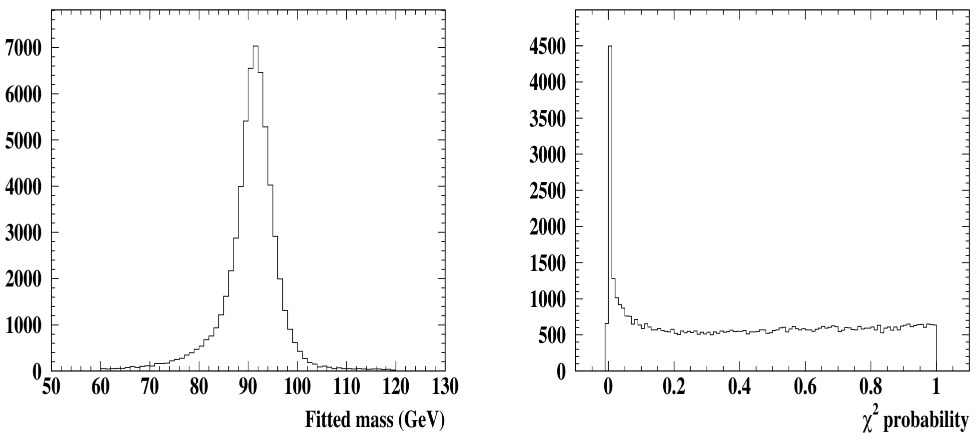

Figure 4: Fitted mass (left) and χ^2 probability (right) resulting from the 1-C fit applied to $ZZ\nu\nu \to q\bar{q}q\bar{q}\nu\bar{\nu}$ events.

The tracks reconstructed in the detector are forced into four jets using the Durham algorithm [13]. The $ZZ\nu\nu$ hypothesis is tested via a kinematic fit to the jet 4-vectors, forcing two jet pairs to have the same mass (1C fit). The resolutions assumed in the fit have been parametrized as a function of the jet masses and azimuthal angles. In figure 4 the fitted mass and the χ^2 probability of the fit are shown, in the case of $ZZ\nu\nu \to q\bar{q}q\bar{q}\nu\bar{\nu}$ events.

The jet pairing is chosen out of the 3 possible combinations using a likelihood discriminant whose inputs are the difference between the two reconstructed di-jet masses, the 1C-fitted mass, and the χ^2 probability of the fit. This method gives a rate of correct pairings of 93% (the rate raises to 99% for the events passing the final selection).
A first series of preselection cuts is applied, to reduce significantly the $q\bar{q}$, $t\bar{t}$, and 4-fermion backgrounds. Then, to separate the double resonant $ZZ\nu\nu$ signal from the 6-fermion background ($WZe\nu$, $WW\nu\nu$, and other non resonant diagrams), a likelihood discriminant is used as selection variable. The following cuts are applied as preselection:

- 200< E_{miss} <650 GeV
- $|\cos(\theta_{P_{miss}})|$ <0.99
- $|\cos(P_{E_{max}})|$ <0.99
- at least two charged tracks per jet are required.

Here P_{Emax} indicates the momentum of the most energetic track in the event and E_{miss}, P_{miss} are the missing energy and momentum of the event. In order to further reduce the $t\bar{t} \to b\bar{b}q\bar{q}l\nu$ background, the event is then rejected if one of the four most energetic charged tracks is isolated (the sum of the energies of the tracks in a 10 degrees cone around the most energetic track is required to be less than 2 GeV). The likelihood discriminant is then calculated from the following input variables:

M_{miss}	$\lvert\cos(\mathrm{P_{E_{max}}})\rvert$
$\lvert\cos(\theta_{\mathrm{P_{miss}}})\rvert$	1C fitted mass
E_{max}	Jet pairing likelihood

where M_{mis} indicates the event missing mass.

Figure 5 shows the distributions of the likelihood variables for signal and background events.

The events with likelihood greater then 0.84 are selected. After the likelihood selection a further cut is applied, requiring both the two reconstructed di-jet masses being between 85 GeV and 100 GeV. The distribution of the likelihood discriminant is shown in Fig 6.(a), while Fig 6.(b) shows the mass distribution of one $q\bar{q}$ pair for the events selected after the likelihood cut.

The results of the selection in terms of efficiency, purity, and expected number of events for an integrated luminosity of 1000 fb^{-1} at $\sqrt{s}$=800 GeV are shown in Table 2.

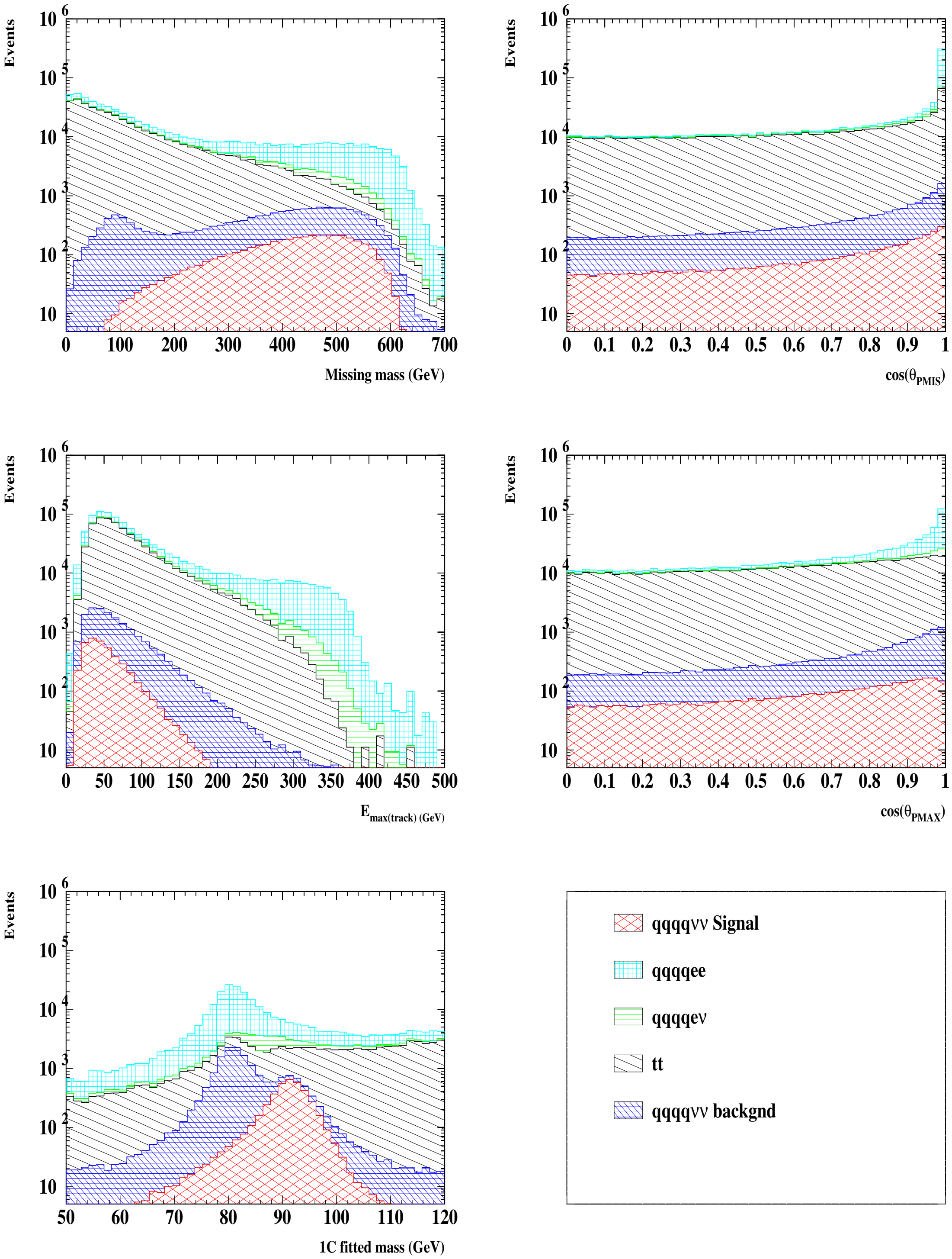

Figure 5: Distributions of the variables used as input for the $ZZ\nu\nu$ likelihood. Shown are the histograms for signal and background.

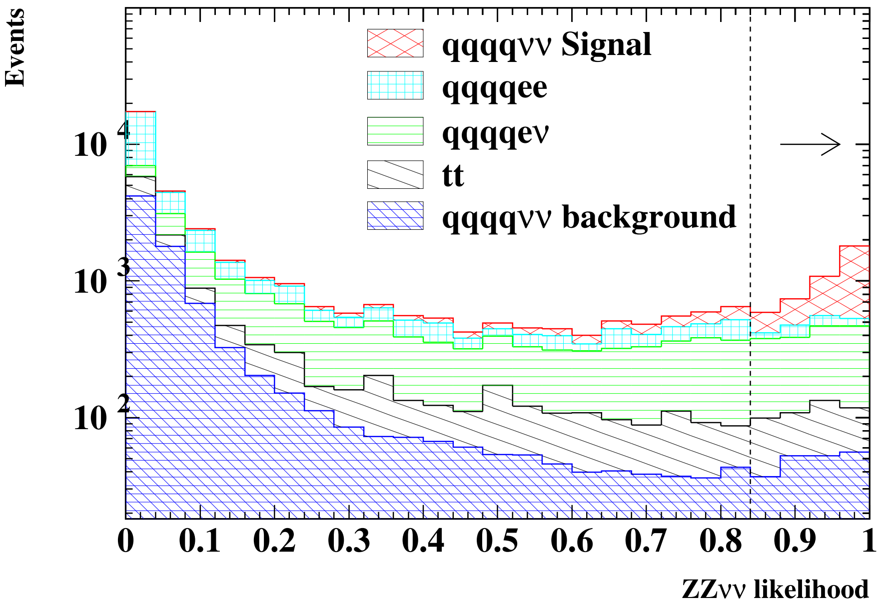

(a)

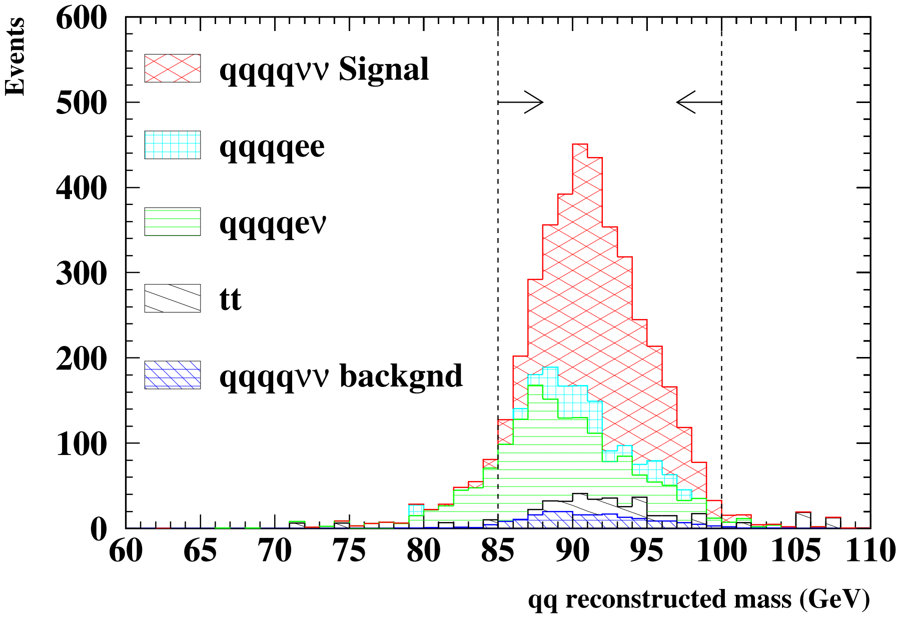

(b)

Figure 6: Likelihood for $ZZ\nu\nu$ selection (a), and mass distribution of one $q\bar{q}$ pair for the events selected after the likelihood cut (b). The histograms are normalised to a total integrated luminosity of 1000 fb^{-1}.

$WW\nu\nu$ selection

To select fully hadronic decays only events with three, four or five jets, reconstructed with the LUCLUS algorithm [6] with d_{join} parameter set to 7 GeV, are selected. Each event is then forced into four jets, where possible, and the jet pairing is chosen in such a way that the product $|m_{ij} - m_W||m_{kl} - m_W|$ is minimum, where m_{ij} and m_{kl} are the jet-jet invariant masses resulting from the pairing. To suppress two and four-fermion contamination and irreducible background coming from ZWW events, with the Z decaying invisibly, the transverse energy in the event, E_{trans}, is required to be in the interval [150 GeV,600 GeV] and the recoil mass, defined as $\sqrt{E_{miss}^2 - p_{miss}^2}$, where E_{miss} and p_{miss} are the missing energy and momentum of the event, to be above 200 GeV. Figure 7 describes the effect of these cuts; the distributions show the two, four and six-fermion components with a normalisation to the chosen luminosity of 1000 fb^{-1}. The cuts are indicated in the picture: the distributions of N_{jet} and E_{trans} are before any other cut, m_{recoil} after having applied the previous two cuts, whereas the distribution of a reconstructed mass shows the final enhancement of the six-fermion component, largely dominated by $WWee$ processes.

To reduce backgrounds leading to isolated leptons in the final state, in particular $t\bar{t}$, the number of charged tracks per forced jet is required to exceed 2. $t\bar{t}$ background is also very much reduced by the rejection of the events with more than 1 tagged b-jet, where the b-tag parametrisation as a function of the jet energy in [14] has been used and the working point with $\epsilon_{b-tag} = 80\%$ chosen. This cut is also effective for $ZZ\nu\nu$ and $WZe\nu$ rejection.
The remaining background comes mainly from six-fermion final states, especially the ones from high cross-section processes like $WWee$ and $WZe\nu$. The characteristic of this background is to have missing momentum, coming from the lost electrons, mostly in the beam pipe. Thanks to an excellent hermeticity and forward coverage they can be very much reduced by a cut on the transverse momentum of the WW system at $p_T^{WW} > 40$ GeV. Also the resolution on the recoil mass benefits from a good hermeticity. The distributions of these two variables are shown, for six fermion final states, in figure 8. The histograms include all the other cuts in the analysis, apart the one on the variable shown.

A further cut to remove combinatorial background and events from the decay of a Z bosons requires both the reconstructed masses to be above 60 GeV and below 88 GeV. Figure 9 shows the final distributions for signal and backgrounds for m_{WW} and m_{qq}, respectively the mass of the WW system and the reconstructed W mass.
Table 2 shows the performance of the analysis in terms of expected number of events, efficiency and remaining backgrounds.

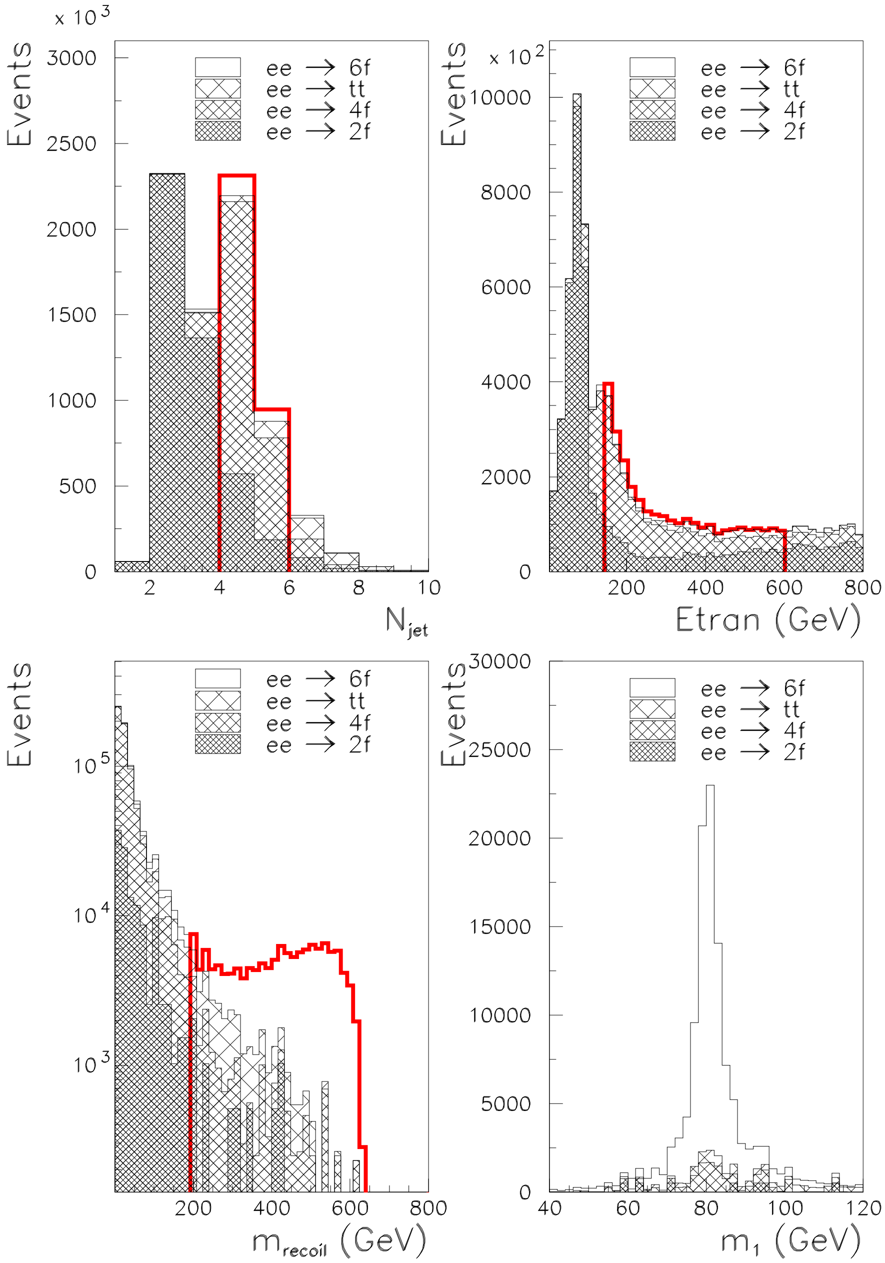

Figure 7: Cuts on number of reconstructed jets, transverse energy and recoil mass to separate between six fermion contributions and other backgrounds. The resulting distribution of one $q\bar{q}$ reconstructed mass is shown.

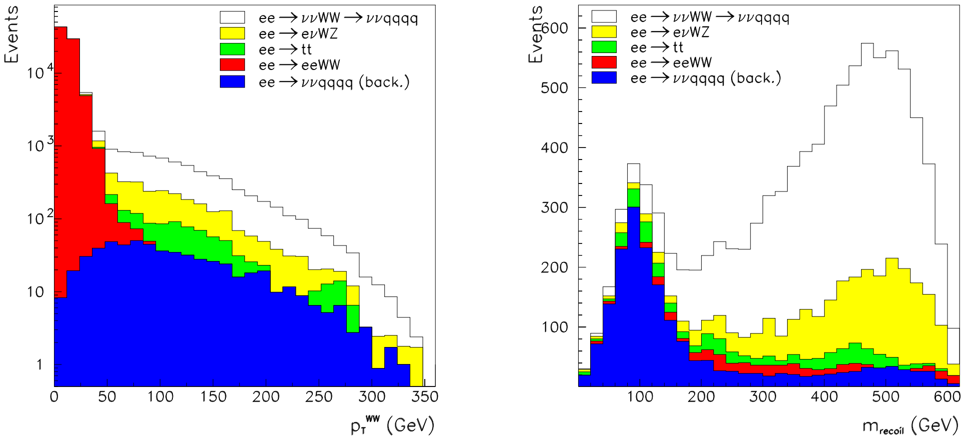

Figure 8: Expected p_T^{WW} (left) and recoil mass (right) distributions for signal and backgrounds, after the application of all the other cuts in the analysis.

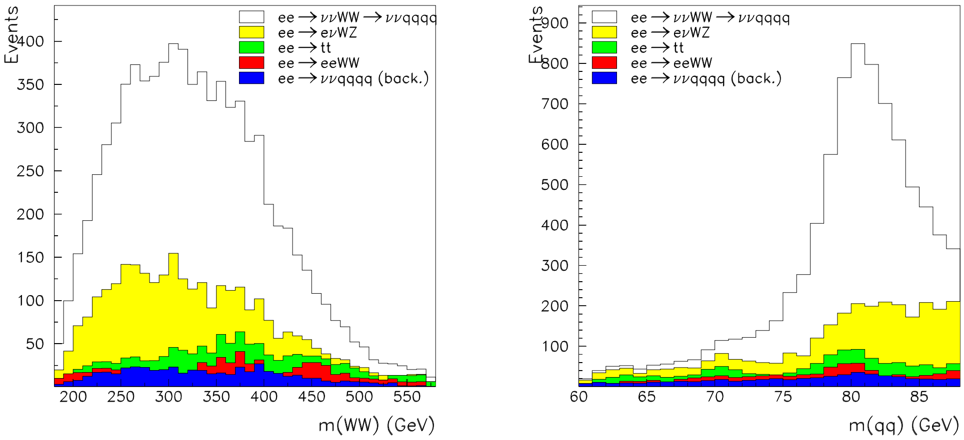

Figure 9: Expected distributions of the WW system mass (left) and the $q\bar{q}$ mass (right) after all the cuts.

Table 2: $ZZ\nu\nu$ and $WW\nu\nu$ selection performance in terms of number of expected events, efficiencies and relative errors on the measured cross-sections. Relative contaminations of $ZZ\nu\nu$ in $WW\nu\nu$ and vice versa are included as $q\bar{q}q\bar{q}\nu\nu$ background.

Channel	Events($ZZ\nu\nu$)	Events($WW\nu\nu$)
$e^+e^- \to ZZ\nu\nu \to q\bar{q}q\bar{q}\nu\nu$	2168±10	
$e^+e^- \to W^+W^-\nu\nu \to q\bar{q}q\bar{q}\nu\nu$		5077±23
$e^+e^- \to q\bar{q}q\bar{q}\nu\nu$ (background)	174±5	509±8
$e^+e^- \to e\nu WZ \to q\bar{q}q\bar{q}e\nu$	993±20	1728±34
$e^+e^- \to W^+W^-e^+e^-, ZZe^+e^- \to q\bar{q}q\bar{q}e^+e^-$	250 ±60	257 ±57
$e^+e^- \to W^+W^-, ZZ \to q\bar{q}q\bar{q}$	negl.	negl.
$e^+e^- \to t\bar{t} \to X$	143±20	444±75
$e^+e^- \to q\bar{q} \to X$	negl.	negl.
efficiency	0.507±0.006	0.588±0.002
$\Delta\sigma/\sigma$	2.8%	1.7%

Fit of the couplings

Signatures of WW strong interactions are changes of the event rate and of the average polarization of the final state bosons with respect to the SM expectation. The total cross section, like the differential cross section at any given point of the phase space, is given by an hyperparaboloid in the (α_4, α_5) space. In figure 10 the ratio of each total cross section to the SM value is shown, versus the coupling values, under the assumption that just one coupling is non-vanishing.

The sensitivity to the anomalous couplings α_4, α_5 is determined by using the total cross section and the distributions of $|\cos(\theta_{W,Z})|$, $|\cos(\theta^*_{decay})|$, and $M_{WW,ZZ}$, where $\theta_{W,Z}$ is the bosons polar angle, θ^*_{decay} is the polar angle of the decay products in the reference frame of each boson, and $M_{WW,ZZ}$ is the event mass (i.e. the mass of the boson pair). No discrimination between quarks and anti-quarks is done. The sensitivity is evaluated through a Binned Maximum Likelihood fit to the expected distributions from a 1000 fb^{-1} SM sample with $\alpha_4 = \alpha_5 = 0$. Figure 11 shows the improvement in the sensitivity obtained by including each of the differential distributions in the likelihood fit. As can be seen, the use of the differential distributions permits to exclude the second intersection between the allowed regions, which appears when looking just at the total cross section.
To evaluate the improvement introduced by the beam polarisation alone, we compared the results of the fit with those of a previous analysis not assuming beam polarisation, as presented in [5]. In the previous analysis the differential distribution $d\sigma/dM_{WW,ZZ}$ had not yet been included in the fit. The comparison is shown in table 3, in terms of one dimensional 68% C.L. limits ($\Delta\chi^2 = 1$) on $\alpha_4,\ \alpha_5$.

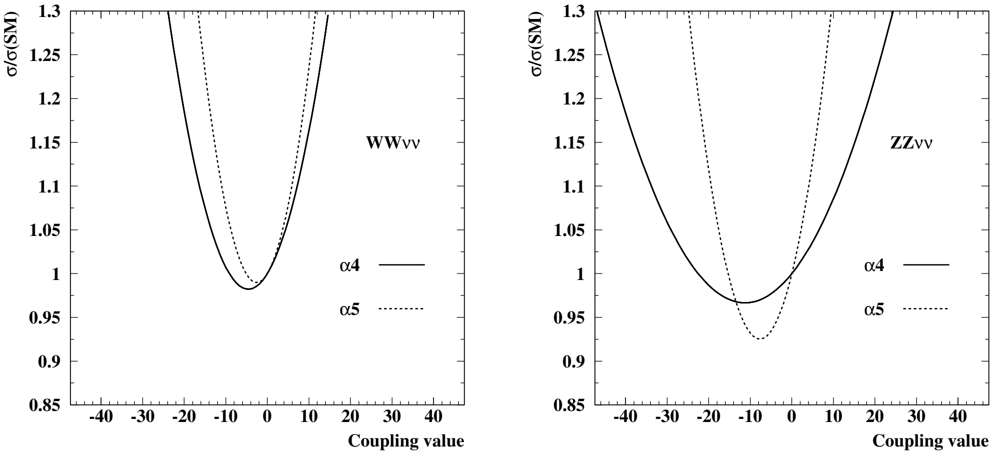

(a) (b)

Figure 10: Ratio between the cross section and the SM value, keeping one coupling at zero and varying the other one, in the case of $WW\nu\nu$ (a), and $ZZ\nu\nu$ (b).

Table 3: Comparison between the analysis presented in [5], where no beam polarisation had been assumed, and the results obtained by this analysis, with beam polarisation. Shown are the one dimensional 68% C.L. ($\Delta\chi^2 = 1$) sensitivities for α_4 and α_5.

No polarisation, $M_{WW,ZZ}$ not in the fit	P_{e^-}=80%, P_{e^+}=40% $M_{WW,ZZ}$ not in the fit	P_{e^-}=80%, P_{e^+}=40% $M_{WW,ZZ}$ in the fit
-1.5< α_4 <1.5 -1.0< α_5 <0.7	-1.3< α_4 <1.0 -0.6< α_5 <0.5	-1.1< α_4 <0.8 -0.4< α_5 <0.3

The results of the fit are shown in figure 12. Figure 12.(a) shows the 68% (continuous line) and 90% (dashed line) C.L. contours obtained by the $WW\nu\nu$ and $ZZ\nu\nu$ analysis respectively, whereas figure 12.(b) shows the C.L. contours obtained from the combination.
As expected, the $ZZ\nu\nu$ sensitivity to the anomalous couplings is better in α_5 than in α_4, whereas for $WW\nu\nu$ the two sensitivities are approximately equivalent. Though the expected cross-section variation with the α's is steeper for the $WW\nu\nu$ final state, from figure 12.a one can appreciate that the final sensitivity of $ZZ\nu\nu$ and $WW\nu\nu$ to the couplings is comparable. The reason for this is that for $WW\nu\nu$ the ratio $\sigma(\alpha_4, \alpha_5)/\sigma(SM)$ is equal to one also for values of the couplings close to

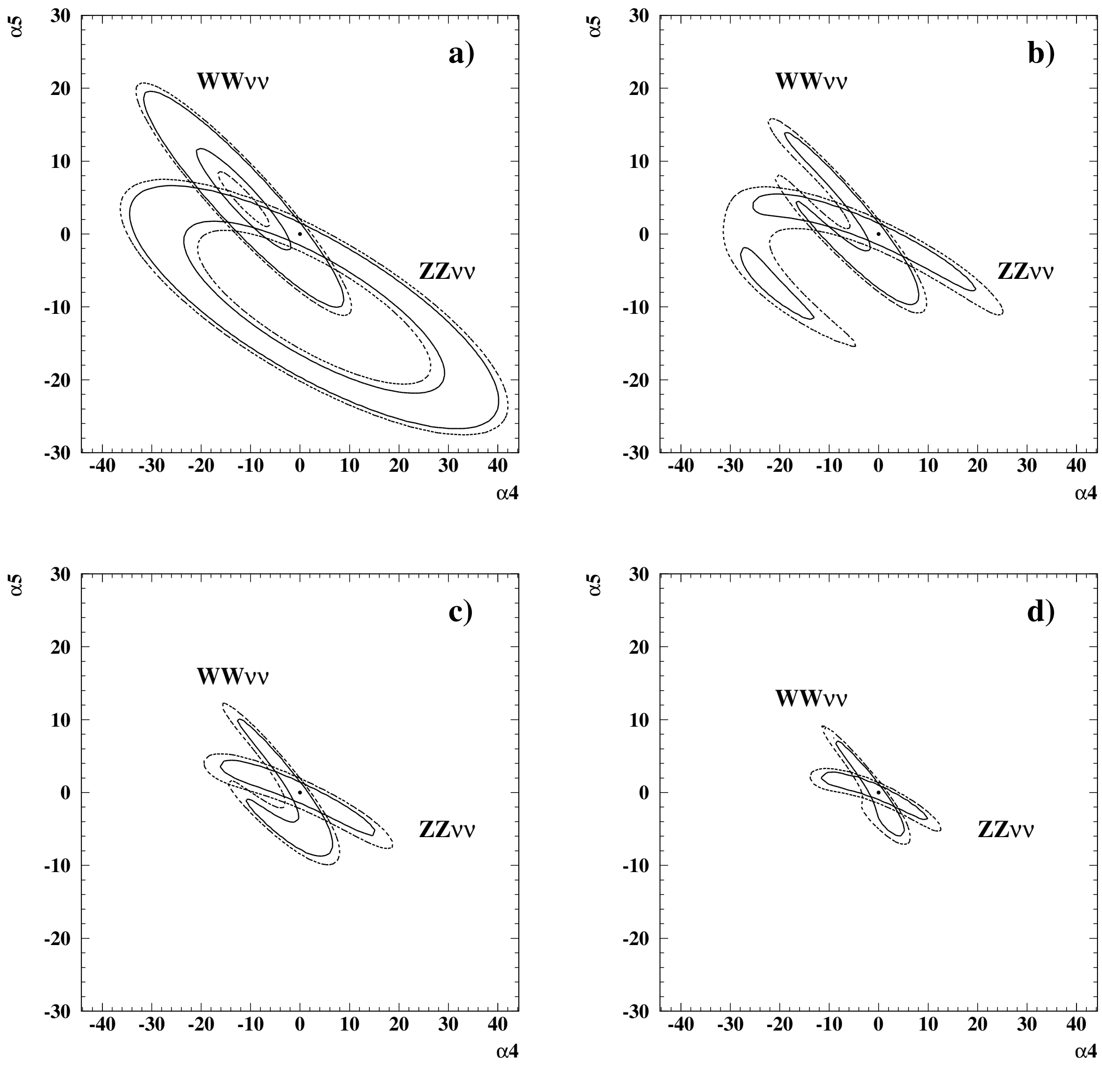

Figure 11: Expected limit contours at 68% (continuous line) and 90% (dashed line) C.L., obtained using in the fit: a) total cross section only; b) including $d\sigma/dcos(\theta_{W,Z})$; c) including $d\sigma/dcos(\theta_{W,Z})$ and $d\sigma/dcos(\theta^*_{decay})$; d) including $d\sigma/dcos(\theta_{W,Z})$, $d\sigma/dcos(\theta^*_{decay})$ and $d\sigma/dM_{WW,ZZ}$, where $M_{WW,ZZ}$ indicates the event mass.

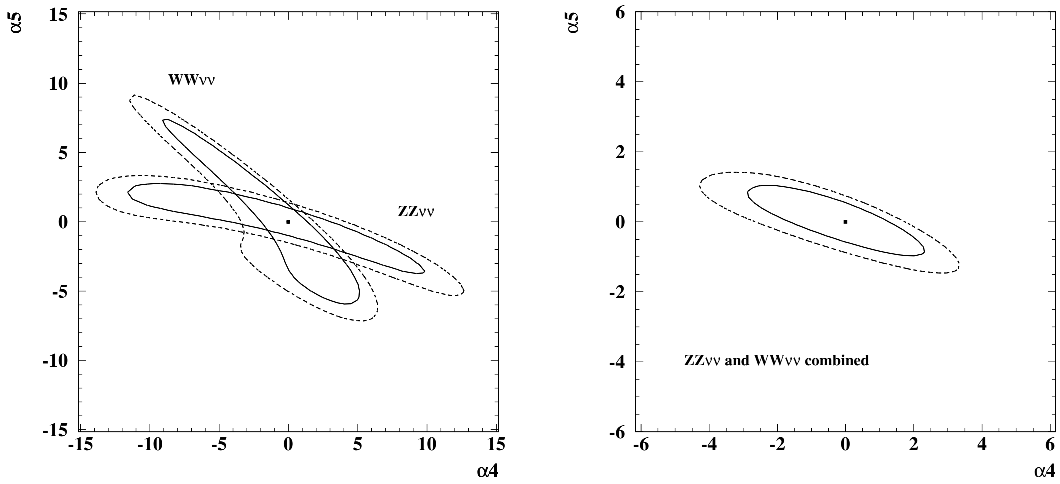

(a) (b)

Figure 12: Expected limit contours on α_4, α_5 for the two analyses (a) and combined limits (b). The continuous lines represent 68% C.L. limits, while the dashed lines are the 90% C.L. limits ($\sqrt{s}$=800 GeV, 1000 fb^{-1}, P_{e^-}=80%, P_{e^+}=40%).

the sensitivity of the analysis (see figure 10). This is not the case for $ZZ\nu\nu$. In this way two non-separable minima appear in the $WW\nu\nu$ likelihood that cause a distortion of its contour and degrade the overall limits. For $ZZ\nu\nu$ the second minimum can be excluded by including in the fit the differential distributions. An increase of the sensitivity should therefore result in a much better improvement on the limits on α_4 and α_5 from $WW\nu\nu$ than from $ZZ\nu\nu$. This can be achieved by studying other decay channels besides the fully hadronic ones, or by increasing the beam polarisations or the integrated luminosity (the limits asymptotically scale as $1/\sqrt{\int \mathcal{L}}$).

Conclusions

The possibility of finding evidence for strong electroweak symmetry breaking signals in WW scattering at TESLA energies with realistic luminosity and beam polarisations has been studied. Detector response and all possible backgrounds have been included in the analyses. The TESLA sensitivity to signals of new physics has been translated into limits on the anomalous couplings α_4 and α_5. Figure 12 shows the expected limit contours in the (α_4, α_5) plane, at 68% and 90% C.L., while Table 4 summarizes the results found in terms of one dimensional 68% C.L. ($\Delta\chi^2 = 1$) sensitivities and compares them with the analogous

68% C.L. $\Delta\chi^2 = 1$	LHC $100\,\mathrm{fb}^{-1}$	TESLA 800 GeV $1000\,\mathrm{fb}^{-1}, P_{\mathrm{e}^-} = 80\%, P_{\mathrm{e}^+} = 40\%$
α_4	$-0.17\ldots+1.7$	$-1.1\ldots+0.8$
α_5	$-0.35\ldots+1.2$	$-0.4\ldots+0.3$
Λ_4^*	2.3 TeV	2.9 TeV
Λ_5^*	2.8 TeV	4.9 TeV

Table 4: Comparison of one dimensional 68% C.L. sensitivities for the strong EWSB parameters (α_4, α_5) at LHC and at a TESLA experiment.

numbers from the LHC [15]. These limits, considerably better than what can be reached at the LHC, are derived from fully hadronic final states only and can therefore be further improved when considering other decay channels with leptons. The limits would also benefit very much from a higher polarisation of the beams, which would increase the signal/background ratio.

References

[1] Timothy L. Barklow et al., *Strong Coupling Electroweak Symmetry Breaking*, in *New Direction For High-Energy Physics*, Proceedings. Edited by D.G. Cassel, L. Trindle Gennari, R.H. Siemann. Stanford, CA, Stanford Linear Accelerator Center, 1997, SLAC-PUB-7397, CLNS-97-1473, hep-ph/9704217

[2] T. Appelquist and C. Bernard, Phys. Rev. **D22** (1980) 200; A. C. Longhitano, Phys. Rev. **D22** (1980) 1166; A. C. Longhitano, Nucl. Phys. **B188** (1981) 118; T. Appelquist and G. Wu, Phys. Rev. **D51** (1995) 240 [hep-ph/9406416].

[3] E. Boos, H. J. He, W. Kilian, A. Pukhov, C. P. Yuan and P. M. Zerwas, Phys. Rev. D **61** (2000) 077901 [hep-ph/9908409]; Phys. Rev. D **57** (1998) 1553 [hep-ph/9708310].

[4] S. Weinberg, Physica **A96** (1979) 327; A. Manohar and H. Georgi, Nucl. Phys. **B234** (1984) 189; H. Georgi and L. Randall, Nucl. Phys. **B276** (1986) 241.

[5] R. Chierici, S. Rosati, M. Kobel, in *Proceedings of the V International e^+e^- Linear Collider Workshop*, Fermilab, 24-28 October 2000.

[6] T. Sjöstrand, *PYTHIA 5.719 / JETSET 7.4*, Physics at LEP2, eds. G. Altarelli, T. Sjöstrand and F. Zwirner, CERN 96-01 (1996) Vol. 2.

[7] W. Kilian, *WHIZARD 1.0: A generic Monte-Carlo integration and event generation package for multi-particle processes*, (see http://www-ttp.physik.uni-karlsruhe.de/Progdata/whizard/), LC-TOOL-2001-039.

[8] T. Ohl, in *Proceedings of 7th International Workshop on Advanced Computing and Analysis Techniques in Physics Research (ACAT 2000)*, [hep-ph/0011243]; in *Proceedings of 5th International Linear Collider Workshop (LCWS 2000)*, [hep-ph/0011287]; M. Moretti, T. Ohl, J. Reuter, *O'Mega: An Optimizing Matrix Element Generator*, (see http://heplix.ikp.physik.tu-darmstadt.de/ ohl/omega/), LC-TOOL-2001-040.

[9] M. Pohl and H. Schreiber, *SIMDET-version 3, a parametric Montecarlo for a TESLA detector*, DESY 99-030, March 1999.

[10] R. Brinkmann, G. Materlik, J. Rossbach and A. Wagner Eds., Conceptual Design of a 500 GeV e^+e^- Linear Collider with Integrated X-ray Laser Facility, DESY 1997-048 and ECFA 1997-182 (1997).

[11] K. Buesser, Proceedings to the V International e^+e^- Linear Collider Workshop, Fermilab, 24-28 October 2000.

[12] T. Ishikawa et al., *GRACE Manual: Version 1.0*, KEK-92-19, Feb 1993.

[13] N. Brown and W.J. Stirling, Phys.Lett.**B252** (1990), 657.

[14] R. Hawkings, *Vertex detector and flavour tagging studies for the TESLA linear collider* LC-PHSM 2000-021/TESLA, February 2000.

[15] A. S. Belyaev et al., *Strongly interacting vector bosons at the CERN LHC: Quartic anomalous couplings* Phys.Rev.**D59**:015022,2000.